HYPERVELOCITY IMPACT PENETRATION PHENOMENA IN ALUMINUM SPACE STRUCTURES

By William P. Schonberg,[1] Associate Member, ASCE

ABSTRACT: All long-duration spacecraft are susceptible to high-speed impacts by meteoroids and pieces of orbiting space debris. Damage to critical spacecraft systems caused by such impacts can lead to spacecraft failure and loss of life. In order to develop adequate protection against penetration for crew compartments and other critical spacecraft systems, an aerospace design engineer must possess a full understanding of the penetration mechanics involved in the hypervelocity impact loading of a variety of structural components. This paper describes the results of an experimental investigation of the penetration phenomena associated with oblique hypervelocity projectile impact of aluminum dual-wall structures. Equations that quantitatively describe these phenomena are obtained through a regression of hypervelocity impact test data. These equations characterize observed penetration phenomena as functions of the geometric and material properties of the impacted structure and the diameter, obliquity, and velocity of the impacting projectile. A review of the test data shows that oblique hypervelocity impact penetration phenomena are strongly dependent on impact obliquity and therefore can differ significantly from those associated with normal high-speed impacts. It is concluded that the possibility of non-normal impacts and their effects on structural integrity must be considered in the design of any structure that is to be exposed to the hazardous meteoroid and space debris environment.

INTRODUCTION

All spacecraft with a mission duration of more than a few days are susceptible to impacts by meteoroids and pieces of space debris. Such impacts are expected to occur at extremely high speeds and are known to produce penetration and ricochet debris. This debris can damage internal as well as external flight-critical systems of the spacecraft, which would lead to catastrophic failure of the spacecraft and loss of life. Therefore, the design of a long-duration spacecraft, such as the space station, must take into account the possibility of such impacts and their effects on the integrity of the entire structural system. Protective systems for habitable compartments and for external structural subsystems must be included in its design.

Protection against penetration for crew compartments and habitable modules has traditionally consisted of a bumper plate that is placed a small distance away from the main structural wall of the compartment or module. This concept was first proposed by Whipple (1947) and has been studied extensively by this writer and other investigators as a means of reducing the penetration threat of hypervelocity impacts (e.g., Schonberg et al. 1988). A thin bumper plate was found to be effective in preventing structural wall penetration because it fragmented an impacting projectile (Wallace 1962; D'Anna 1965; Lundeberg et al. 1965). At sufficiently high velocities, the bumper plate should serve to melt or even completely vaporize the projectile (Maiden and McMillan 1964; Wilkinson 1968; Swift 1983). In this manner,

[1]Asst. Prof., Dept. of Mech. Engrg., The Univ. of Alabama in Huntsville, Huntsville, AL 35899.

Note. Discussion open until December 1, 1990. To extend the closing date one month, a written request must be filed with the ASCE Manager of Journals. The manuscript for this paper was submitted for review and possible publication on July 25, 1989. This paper is part of the ***Journal of Aerospace Engineering***, Vol. 3, No. 3, July, 1990. ©ASCE, ISSN 0893-1321/90/0003-0173/$1.00 + $.15 per page. Paper No. 24805.

whatever parrticles do strike the main pressure wall will have little, if any, penetrating power. In the design process, bumper and pressure wall thicknesses are iterated against weight and protection considerations to arrive at a final configuration. For a more detailed description of the processes involved in normal hypervelocity projectile impact, the reader is referred to proceedings of hypervelocity impact symposia held in the late 1950s and early 1960s as well as Kinslow (1970) and Zukas et al. (1982).

In the majority of such prior investigations, the trajectories of the projectiles were normal to the surfaces of the impacted structures. However, it has become evident that most meteoroid and space debris impacts will not occur normal to the surface of a spacecraft (Coronado et al. 1987). In a preliminary investigation of oblique hypervelocity impact (Schonberg and Taylor 1989), a rudimentary set of predictor equations was developed to characterize quantitatively various oblique penetration phenomena. The existence of a critical value of impact trajectory obliquity was documented and was shown to be a significant factor in determining whether the structural wall of the test specimen was penetrated by the projectile or its fragments. It was demonstrated that if a projectile with an impact obliquity less than the critical angle would penetrate the pressure wall, then a projectile of similar impact energy with a trajectory obliquity greater than the critical value would produce only a minimal amount of crater damage on the pressure wall plate of a similar test specimen. This critical angle was estimated to have a value between 60° and 65°. However, the test program conducted for that study was limited in scope and did not consider a very wide variety of projectile diameters, angles of obliquity, and test specimen configurations.

The objectives of the present investigation are as follows: (1) To supplement the current hypervelocity impact test data base with data from new oblique and normal test firings; (2) to extend the applicability of the empirical equations developed in the initial oblique hypervelocity impact study to a greater variety of structural wall systems and impact parameters; and (3) to develop additional empirical predictor equations for phenomena not considered in the initial investigation. In the first section of this paper, the experimental procedure used in the oblique hypervelocity impact testing of dual-wall specimens is reviewed. In the next section, the penetration processes associated with oblique hypervelocity impact of dual-wall structures are described qualitatively. In the following sections, new empirical equations quantifying the response of dual-wall structures to oblique hypervelocity impact are presented and discussed.

Experimental Procedure and Results

The oblique hypervelocity impact testing of multi-sheet specimens was performed at the Space Debris Simulation Facility of the Materials and Processes Laboratory at the Marshall Space Flight Center (Taylor 1987). The facility consists of a light gas gun with a 12.7-mm launch tube capable of launching 2.5–12.7 mm diameter projectiles of mass 4–300 mg at velocities of 2–8 km/s. Projectile velocity measurements were accomplished via pulsed X-ray, laser diode detectors, and a Hall photographic station. A drawing of a typical multi-sheet specimen setup is shown in Fig. 1.

In each test, a spherical projectile of diameter D and velocity V impacted a bumper plate of thickness t_s at an angle of obliquity θ. The projectile was

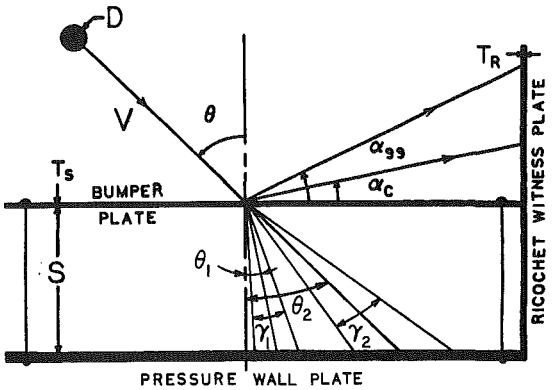

FIG. 1. Test Configuration and Parameter Definitions

TABLE 1. Impact Test Data: Penetration Angles

Test number (1)	V (km/s) (2)	d (mm) (3)	θ (degrees) (4)	θ_1 (degrees) (5)	θ_2 (degrees) (6)	γ_1 (degrees) (7)	γ_2 (degrees) (8)
EH1A	7.07	7.95	30	—	24.8	—	56.3
EH1B	6.96	7.95	45	10.9	38.1	42.3	30.7
EH1C	7.14	7.95	60	9.6	50.0	46.6	16.9
EH1D	7.18	7.95	75	4.7	26.9	57.1	—
EHAP	6.82	7.95	75	5.0	22.0	55.7	—
EHAA	6.93	7.95	75	4.7	22.2	47.8	—
EHAB	6.91	7.95	75	5.0	19.9	55.9	—
EHBP	7.22	6.35	75	4.3	21.8	48.7	—
EHCP	7.58	4.75	75	4.7	20.9	38.6	—
1061	6.84	8.89	60	11.3	47.1	43.4	26.5
106A	6.66	9.53	60	9.2	48.4	47.4	16.9
135C	6.76	6.35	30	—	24.0	—	53.0
135D	6.93	6.35	30	—	27.0	—	53.3
136A	6.25	6.35	55	10.7	43.5	43.9	20.9
136B	7.30	6.35	55	10.1	41.8	41.7	23.5
136C	6.67	6.35	55	11.0	38.2	44.5	24.3
150A	7.08	6.35	45	10.0	39.0	39.6	28.4
157A	7.40	4.75	60	9.3	36.0	42.4	21.2
162A	6.49	4.75	30	—	21.0	—	64.8
162B	5.03	4.75	30	—	27.0	—	52.7
206F	6.24	4.75	45	8.0	31.0	29.4	31.0
208E	6.48	6.35	65	9.0	47.0	43.5	11.7
209D	7.40	6.35	65	—	—	—	—
230C	5.16	6.35	45	10.0	34.0	34.3	23.7
230D	5.59	6.35	45	10.0	37.0	34.8	24.8
230E	6.62	6.35	45	10.0	32.0	33.0	28.3
231C	6.59	7.95	65	8.7	55.7	47.1	10.2
231D	7.26	7.95	65	10.2	49.7	48.5	20.1
EHRP1	6.87	7.95	60	10.6	46.5	52.9	22.6
EHRP2	6.80	7.95	65	11.0	64.4	49.3	9.4

TABLE 2. Impact Test Data: Bumper Plate Hole Dimensions

Test number (1)	V (km/s) (2)	d (mm) (3)	θ (degrees) (4)	D_{min} (mm) (5)	D_{max} (mm) (6)	Eccentricity (7)	D (mm) (8)
EH1A	7.07	7.95	30	16.0	17.0	1.06	—
EH1B	6.96	7.95	45	16.5	20.0	1.22	—
EH1C	7.14	7.95	60	16.5	24.9	1.51	—
EH1D	7.18	7.95	75	14.5	36.1	2.49	—
EHAP	6.82	7.95	75	13.0	33.0	2.53	—
EHAA	6.93	7.95	75	13.2	33.5	2.54	—
EHAB	6.91	7.95	75	13.2	33.5	2.54	—
EHBP	7.22	6.35	75	10.9	23.1	2.09	—
EHCP	7.58	4.75	75	10.0	18.0	1.82	—
006A	6.95	6.35	0	—	—	1.00	15.0
013B	6.15	6.35	0	—	—	1.00	14.0
033	7.21	6.35	0	—	—	1.00	13.2
033C	5.53	6.35	0	—	—	1.00	11.2
035C	5.72	8.89	0	—	—	1.00	16.0
102	7.20	7.62	0	—	—	1.00	18.0
1061	6.84	8.89	60	18.8	29.0	1.54	—
106A	6.66	9.53	60	19.8	32.5	1.64	—
107B	6.82	8.89	0	—	—	1.00	18.5
135C	6.76	6.35	30	13.2	14.2	1.08	—
135D	6.93	6.35	30	13.2	14.2	1.08	—
136A	6.25	6.35	55	14.0	18.3	1.31	—
136B	7.30	6.35	55	14.0	20.1	1.44	—
136C	6.67	6.35	55	13.5	17.0	1.26	—
150A	7.08	6.35	45	14.2	18.0	1.26	—
157A	7.40	4.75	60	13.7	17.3	1.26	—
162A	6.49	4.75	30	11.9	14.0	1.18	—
162B	5.03	4.75	30	9.9	11.7	1.17	—
206F	6.24	4.75	45	11.7	13.5	1.16	—
208E	6.48	6.35	65	13.0	21.0	1.61	—
209D	7.40	6.35	65	14.5	19.6	1.36	—
213B	5.90	7.95	0	—	—	1.00	16.5
228B	6.75	7.95	0	—	—	1.00	12.7
228D	6.65	6.35	0	—	—	1.00	11.2
230C	5.16	6.35	45	12.4	16.0	1.28	—
230D	5.59	6.35	45	13.5	16.3	1.22	—
230E	6.62	6.35	45	14.2	17.5	1.25	—
231C	6.59	7.95	65	16.5	31.0	1.87	—
231D	7.26	7.95	65	16.5	25.9	1.57	—
EHRP1	6.87	7.95	60	16.5	29.0	1.74	—
EHRP2	6.80	7.95	65	16.0	33.0	2.19	—

shattered upon impact and created an elliptical hole in the bumper plate. Some secondary projectile and bumper plate fragments were sprayed upon the pressure wall plate a distance S away, while some fragments riocheted and struck the ricochet witness plate. The angles θ_1 and θ_2 denote the trajectories of the centers of mass of bumper and "in-line" penetration fragments, respectively; the angles γ_1 and γ_2 represent the spread of these frag-

ments. The angles α_c and α_{99} characterize the trajectories of the ricochet fragments.

The configurations of the test specimens and the conditions of impact were chosen to simulate the conditions of space debris impact as closely as possible and still remain within the realm of experimental feasibility. Kessler (1989) states that the average mass density for pieces of orbital space debris less than 10 mm in diameter is approximately 2.8 gm/cm^3, which is approximately the same as the density of aluminum. Thus, the projectiles used were solid 1100 aluminum spheres with diameters ranging from 4.75 mm to 9.2 mm. The bumper, pressure wall, and ricochet witness plates were made of 6061-T6, 2219-T87, and 2219-T87 aluminum, respectively. The thicknesses of the bumper plates were varied from 0.8128 mm to 2.032 mm; that of the pressure wall plate was held constant at 3.175 mm. The bumper and pressure wall plates were separated by a constant distance of 101.6 mm. The obliquity of the impact was varied from 0° to 75°, while the impact velocities ranged from 5.0 to 8.0 km/s. Based on these parameters, the predictor equations subsequently developed strictly are valid for aluminum projectiles and bumper plates and for $0.0853 < t_s/d < 0.4278$.

Thirty oblique and 10 normal tests were used to study hypervelocity impact penetration phenomena. The data derived from these tests are presented in Tables 1 and 2. In Table 1, the angles θ_1 and θ_2 were obtained by estimating the locations of the centers-of-mass of the crater clusters caused by bumper plate fragment and "in-line" projectile fragment impact on the pressure wall plate; the cone angles γ_1 and γ_2 were obtained by measuring the width of the damage clusters in the direction of impact. In Table 2, the minimum and maximum dimensions of the bumper plate holes in the oblique impacts and the hole diameters for normal impacts were measured directly from the bumper plates.

Oblique Hypervelocity Impact Process

The formation and growth of penetration and ricochet debris clouds are clearly visible in Figs. 2 through 5. These figures show the various stages of the oblique impact process beginning with a pre-event photograph (Fig. 2). As the projectile strikes the bumper plate, the projectile and the portion of the bumper plate surrounding the site of impact shatter into many fragments. In Fig. 3, a ricochet debris cloud consisting of projectile and plate fragments is seen to be the first to form. The penetration debris cloud is subsequently produced by further plate fragmentation. Its motion is initially directed along the outward normal of the reverse side of the plate (Fig. 4). The impact event progresses and the remainder of the projectile fragments exit the rear of the plate. The penetration debris cloud then acquires an additional component of motion parallel to the rear surface of the plate. The net result is that the penetration debris cloud begins to move in a direction similar to that of the original projectile (Fig. 5).

When the angle of obliquity is 45° or less, there is extensive penetration damage to the pressure wall plate. This damage is typically in the form of one or more large holes whose circumferences are jagged and petaled. Only a relatively small quantity of ricochet debris is formed in such impacts. For trajectory obliquities greater than 45° but less than the critical angle, two distinct areas of damage are usually formed on the pressure wall plate. In

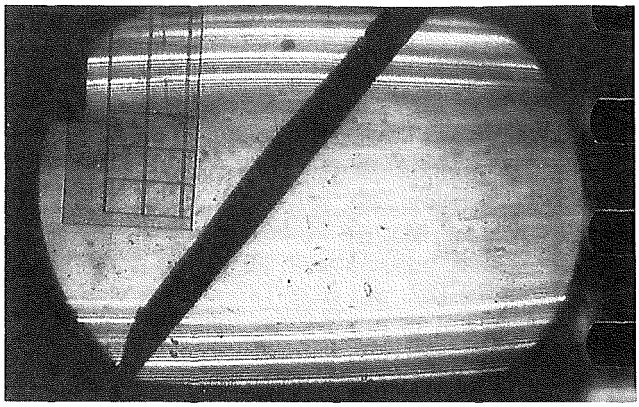

FIG. 2. Oblique Hypervelocity Impact: Pre-Event Stage ($V \sim 6$ km/s, $\theta = 45°$, $t_s/d \sim 3$)

one damage zone, the craters and holes are nearly circular, which is characteristic of near-normal impact. In the other, the craters are oblong, indicating that they are formed by oblique impacts. From such observations it is possible to differentiate between pressure wall damage caused by bumper plate fragments and that caused by projectile fragments. The bumper plate fragments travel along a near-normal path between the bumper plate and the pressure wall plate and therefore produce the circular holes and craters. The projectile fragments travel along a trajectory "in-line" with the original projectile trajectory, thereby producing the oval craters and holes. These observations confirm the findings of an early investigation of oblique hypervelocity impact phenomena by Burch (1967).

As the trajectory obliquity is increased beyond 45°, a significant amount of ricochet debris is produced by the impact. Once the critical value of im-

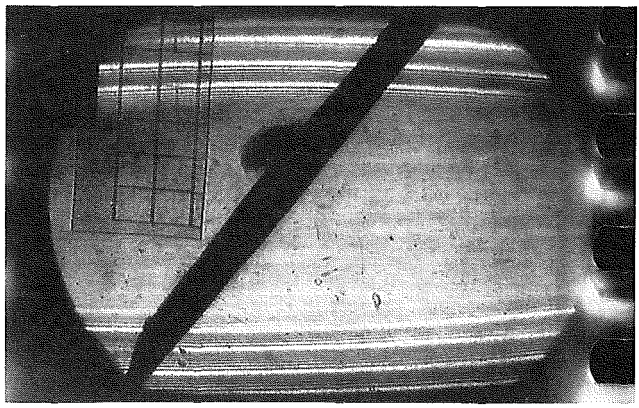

FIG. 3. Oblique Hypervelocity Impact: Formation of Ricochet Debris Cloud ($V \sim 6$ km/s, $\theta = 45°$, $t_s/d \sim 3$)

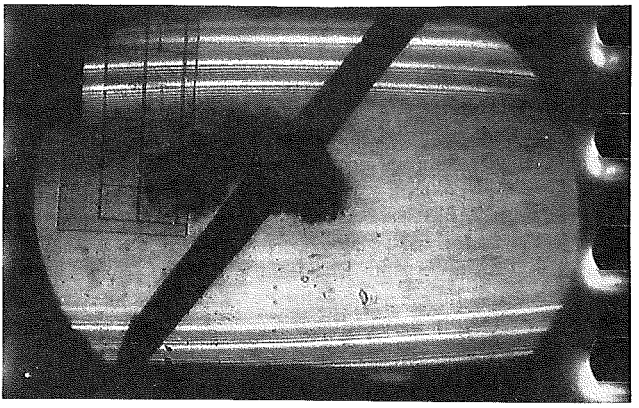

FIG. 4. Oblique Hypervelocity Impact: Formation of Penetration Debris Cloud ($V \sim 6$ km/s, $\theta = 45°$, $t_s/d \sim 3$)

pact obliquity is exceeded, the penetration damage inflicted on the pressure wall by bumper plate and projectile fragments decreases dramatically. Impacts with trajectory obliquities beyond 60° or 65° produce a tremendous amount of ricochet debris and only a small quantity of "penetration" debris. Photographs of damaged pressure wall and ricochet witness plates illustrating these phenomena may be found in Coronado et al. (1987) and in Schonberg et al. (1988).

These observations reveal that for trajectory obliquities below 30° and above 65° there is significant overlapping of the projectile and bumper plate debris clouds. At intermediate obliquities, whether there is any separation of the debris clouds depends on the original impact parameters. It is interesting to note that in the case of low-trajectory obliquity, the overlapping of the debris clouds concentrates the debris into a much smaller volume and thereby in-

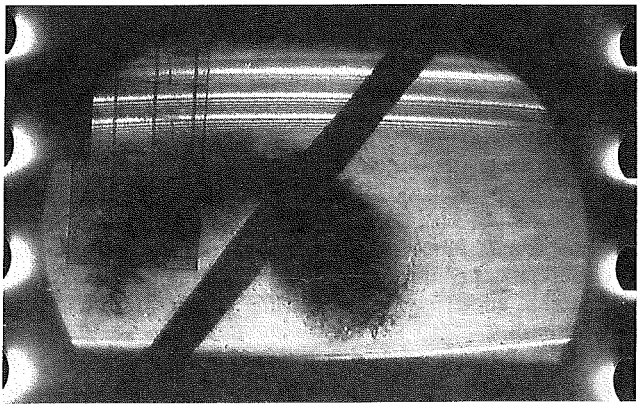

FIG. 5. Oblique Hypervelocity Impact: Spread of Ricochet and Penetration Debris Clouds ($V \sim 6$ km/s, $\theta = 45°$, $t_s/d \sim 3$)

creases the damage potential of the projectile and bumper plate debris particles. However, in the high-obliquity regime, because so few penetration particles are created, the overlapping of the debris clouds does not contribute significantly to their damage potential.

Bumper Plate Hole Analysis

In order to estimate the damage potential of the penetration fragments, it is necessary to know the total volume of debris generated by the impact. A good estimate of the bumper plate fragment volume can be obtained by multiplying the area of the hole formed during the impact by the thickness of the bumper plate. Inspection of obliquely impacted test specimens revealed the bumper plate holes to be elliptical, with the elongations in the directions of the original projectile trajectories. In these cases, the bumper plate hole areas can be approximated as those of ellipses with major and minor axes equal to the maximum and the minimum hole dimensions. In the cases of normal impact, the bumper plate holes are circular, with equal maximum and minimum hole dimensions.

Although the smaller hole dimension, D_{min}, was previously observed by Schonberg and Taylor (1989) to be independent of obliquity, inspection of the bumper plate holes in new test specimens revealed an increasing dependence on obliquity, especially in the high-obliquity test specimens. Furthermore, the original equations for the maximum dimension of the bumper plate hole, D_{max}, did not correlate well with experimental data for very large angles of obliquity. The objectives of the analyses in this task were to: (1) Modify the existing equation for D_{min} by including a dependence on trajectory obliquity; and (2) improve the accuracy of the current equation for D_{max}, especially in the high-obliquity regime. In addition, the applicability of both equations was extended by including normal impact data in the derivation of the hole dimension predictor equations. These equations were obtained through a multiple linear regression of the hole dimension data with the following results:

$$\frac{D_{min}}{d} = 2.825\left(\frac{V}{C}\right)^{1.043} \cos^{0.283}\theta\left(\frac{t_s}{d}\right)^{0.782} + 1.01 \qquad 0° < \theta < 75° \quad \ldots\ldots\ldots (1)$$

$$\frac{D_{max}}{d} = 1.250\left(\frac{V}{C}\right)^{0.851} e^{1.064\theta}\left(\frac{t_s}{d}\right)^{0.672} + 1.40 \qquad 0° < \theta < 75° \quad \ldots\ldots\ldots\ldots (2)$$

where C = the speed of sound in the bumper plate material; and Θ is in radians. The averages and standard deviations of the prediction errors of the regression equations are presented in section *a* of Table 3 (columns 2 and 3, respectively). A measure of the accuracy of the regression equations, the correlation coefficient, is presented for each equation in column 4. It can be seen from this table and from Fig. 6 that the equations are a fairly good fit to the hole dimension data. The relatively large spread of the prediction errors for Eq. 2 is due to an inherent physical uncertainty in the maximum hole dimension, especially in holes produced by high-obliquity impacts. High-obliquity impact will tear, as well as perforate, the bumper plate in the direction of the line of flight of the projectile. The effects of this tearing process on the maximum hole dimension were found to vary dramatically, even

TABLE 3. Regression Analysis Error Summary

Equation (1)	% ϵ_{avg} (2)	σ (%) (3)	$100R^2$ (4)
(*a*) Hole Dimension Predictor Equations			
1	0.001	6.550	72.3
2	0.055	11.410	86.1
(*b*) Empirical Expressions for θ_1 and θ_2			
4	0.612	11.029	94.8
5	2.209	21.436	73.9
(*c*) Debris Cloud Cone Angle Equations			
6	0.187	6.261	73.8
7	2.515	22.436	92.5

between similar impact test shots (note the difference in D_{max} for tests 231C and 231D). It is also interesting to note that the coefficients and exponents of Eq. 1 are very close to the corresponding constants in the equation obtained by Maiden et al. (1963) for hole diameters in thin plates under normal high-speed impact

$$\frac{D}{d} = 2.40\left(\frac{V}{C}\right)^{0.666} + 0.90 \quad \text{(3)}$$

where D = the diameter of the (circular) hole in the bumper plate.

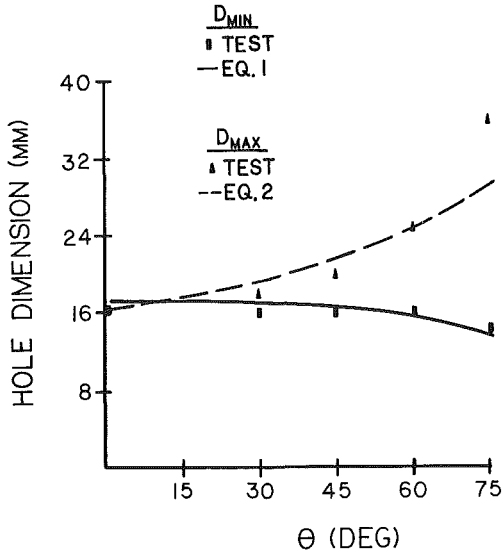

FIG. 6. Bumper Plate Hole Dimensions: Test Data Compared to Regression Equation Predictions ($V \sim 7$ km/s, $d = 7.95$ mm)

PENETRATION DEBRIS CENTER-OF-MASS TRAJECTORY ANALYSIS

As in the case of the hole dimension equations, the equations for θ_1 and θ_2 obtained previously were improved by including the data from the new test specimens in the regression data base. Empirical expressions for θ_1 and θ_2 were obtained as functions of projectile diameter, impact velocity, and trajectory obliquity with the following results:

$$\frac{\theta_1}{\theta} = 0.184\left(\frac{V}{C}\right)^{0.290} \cos^{1.372}\theta\left(\frac{t_s}{d}\right)^{-0.488} \qquad 45° < \theta < 75° \ldots\ldots\ldots\ldots\ldots \quad (4)$$

$$\frac{\theta_2}{\theta} = 0.490\left(\frac{V}{C}\right)^{-0.056} \cos^{0.909}\theta\left(\frac{t_s}{d}\right)^{-0.626} \qquad 30° < \theta < 75° \ldots\ldots\ldots\ldots\ldots \quad (5)$$

The averages and standard deviations of the prediction errors and the correlation coefficients for each equation are presented in section *b* of Table 3. The somewhat large spread of the prediction errors for these equations is probably present because it was often difficult to determine the exact boundaries and centers of the "normal" and "in-line" debris crater clusters. The actual values of the penetration angles are therefore seen to depend somewhat on the person performing the analyses. However, these equations are more compact and have a higher correlation with experimental results than the equations previously developed.

A comparison of predicted and actual values of θ_1 and θ_2 is presented in Fig. 7. It is seen that the "in-line" trajectory angle, θ_2, is not a single-valued function of trajectory obliquity. In fact, θ_2 varies directly with θ up to a critical value between 60° and 65° and then decreases with further increases in θ. This reversal at the critical value of trajectory obliquity also corre-

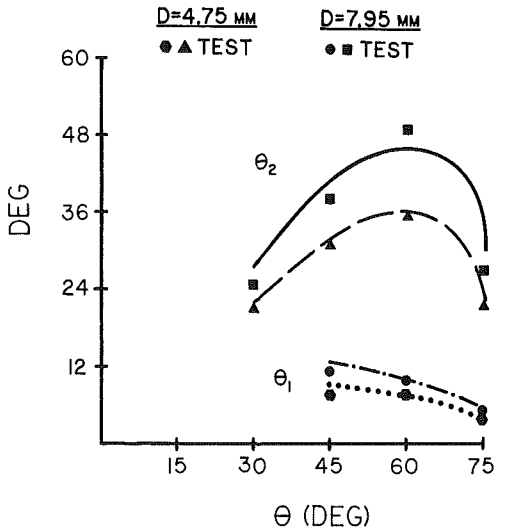

FIG. 7. Penetration Fragments Trajectories: Test Data Compared to Regression Equation Predictions ($V \sim 7$ km/s, $d = 7.95$ mm)

sponds to the sudden decrease in the penetration potential of a high-speed projectile.

Penetration Debris Cloud Cone Angles

In an effort to assess the extent of penetration damage as well as location, equations relating the spread of the projectile and bumper plate penetration debris were developed. These equations could be used with the center of mass trajectory equations to assess whether the debris clouds formed as the result of an oblique impact would overlap and concentrate their energy or separate and distribute their energy upon the pressure wall plate. Debris cloud cone angle equations were obtained using standard multiple linear regression techniques with the following results:

$$\frac{\gamma_1}{\theta} = 0.417\left(\frac{V}{C}\right)^{0.228} \cos^{0.225}\theta\left(\frac{t_s}{d}\right)^{-0.491} \qquad 45° < \theta < 75° \quad \ldots\ldots\ldots\ldots\ldots (6)$$

$$\frac{\gamma_2}{\theta} = 2.539\left(\frac{V}{C}\right)^{1.217} \cos^{2.972}\theta\left(\frac{t_s}{d}\right)^{0.296} \qquad 30° < \theta < 65° \quad \ldots\ldots\ldots\ldots\ldots (7)$$

It is noted that the regions of applicability of the cone angle equations are indicative of the overlapping phenomena for low- and high-trajectory obliquities. The averages and standard deviations of the prediction errors and the correlation coefficients for Eqs. 6 and 7 are presented in section *c* of Table 3, where it is seen that the equations are a fairly good fit to the cone angle data.

Conclusions

An investigation of the penetration processes in oblique hypervelocity projectile impact has been performed. The important characteristics of the penetration process are summarized in this section. These observations must be considered in the design of spacecraft, such as the space station, that are developed for long-duration missions in the meteoroid and space debris environments.

There exists a critical value of impact obliquity. Projectiles with impact obliquities less than this critical value can produce significant penetration damage to the pressure wall of a spacecraft, while projectiles with trajectory obliquities greater than the critical value typically cause minimal penetration damage. This critical angle is estimated to have a value between 60° and 65°. The existence of such an angle is expected to have serious consequences on the development of protective shielding for the habitable compartments of a spacecraft and on the design and placement of its external subsystems, such as solar arrays and instrumentation units.

Low-obliquity hypervelocity impacts are potentially more dangerous to pressurized spacecraft modules than normal impacts with otherwise similar characteristics. In a low-obliquity impact, the projectile and bumper plate debris clouds overlap and combine to form a single, more concentrated debris cloud than that formed in a normal impact. Even a small-trajectory obliquity has been found to be sufficient in concentrating the kinetic energies of the debris particles so as to cause penetration of the pressure wall.

High-obliquity impacts have a lower penetration potential for pressure wall penetration than low-obliquity impacts for two reasons. First, the quantity of projectile and bumper plate debris created in high-obliquity impacts is much lower than the quantity of debris created in low-obliquity impacts. Second, the bumper plate debris and projectile debris clouds can separate in a high-obliquity impact, which serves to dissipate the kinetic energy of the debris particles.

Empirical equations that can be used to estimate the location and the extent of penetration damage were developed based on debris cloud angle data. These equations are naturally limited to the range of impact and geometric parameters considered in this investigation. These equations can also be used to determine whether the bumper plate and projectile debris clouds will overlap and combine their penetrating potentials or separate and dissipate their kinetic energies. However, it should be noted that high-obliquity impacts have a very high potential for damage to external spacecraft systems because of the large volume of ricochet debris particles that they produce.

Acknowledgments

The writer wishes to acknowledge the support of the NASA/ASEE Summer Faculty Fellowship Program along with Michael Freeman, the University of Alabama Director, and Ernestine Cothran, the MSFC Program Co-director. The writer wishes to express his appreciation to Roy Taylor, Chief of the Laboratory Support Branch, for his suggestions during the course of the investigation, and to Hubert Smith of the Laboratory Support Branch for conducting the impact testing that made this report possible. The writer's gratitude is also extended to Jane Schonberg for her assistance in the preparation of this manuscript and to the NASA Johnson Space Center for providing the high-speed photographs of the oblique impact process.

Appendix I. References

Burch, G. T. (1967). "Multi-plate damage study." *Report No. AFATL-TR-67-116,* Air Force Armament Lab., Eglin Air Force Base, Fla.

Coronado, A. R., et al. (1987). "Space station integrated wall design and penetration damage control." *Report No. D180-30550-1,* Contract NAS8-36426, Boeing Aerospace Co., Seattle, Wash.

Cour-Palais, B. G. (1979). "Space vehicle meteoroid shielding design." *Proc., Comet Halley Micrometeoroid Hazard Workshop,* European Space Agency Special Publication No. 153, 89–92.

D'Anna, P. J. (1965). "A combined system concept for control of the meteoroid hazard to space vehicles." *J. Spacecraft,* 2(1), 33–37.

Kessler, D. J. (1989). "Orbital environment for spacecraft designed to operate in low earth orbit." *NASA TM-100471,* Washington, D.C.

Kinslow, R. (1970). *High velocity impact phenomena.* Academic Press, New York, N.Y.

Lundeberg, J. F., Stern, P. H., and Bristow, R. J. (1965). "Meteoroid protection for spacecraft structures." *NASA CR-54201,* Washington, D.C.

McMillan, A. R. (1968). "Experimental investigations of simulated meteoroid damage to various spacecraft structures." *NASA CR-915,* Washington, D.C.

Maiden, C. J., Gehring, J. W., and McMillan, A. R. (1963). "Investigation of fundamental mechanism of damage to thin targets by hypervelocity projectiles." *GM-DRL-TR-63-225,* General Motors Defense Res. Lab., Santa Barbara, Calif.

Maiden, C. J., and McMillan, A. R. (1964). "An investigation of the protection

afforded a spacecraft by a thin shield." *AIAA J.*, 2(11), 1992–1998.
Schonberg, W. P., and Taylor, R. A. (1989). "Penetration and ricochet phenomena in oblique hypervelocity impact." *AIAA J.*, 27(5), 639–646.
Schonberg, W. P., Taylor, R. A., and Horn, R. A. (1988). "An analysis of penetration and ricochet phenomena in oblique hypervelocity impact." *NASA TM-100319*, Washington, D.C.
Swift, H. F., Bamford, R., and Chen, R. (1983). "Designing space vehicle shields for meteoroid protection: A new analysis." *Adv. Space Res.*, 2(12), 219–234.
Taylor, R. A. (1987). "A space debris simulation facility for spacecraft materials evaluation." *SAMPE Quarterly*, 18(2), 28–34.
Wallace, R. R., Vinson, J. R., and Kornhauser, M. (1962). "Effects of hypervelocity particles on shielded structures." *ARS J.*, 32(8), 1231–1237.
Whipple, E. L. (1947). "Meteorites and space travel." *Astronomical J.*, 52, 131.
Wilkinson, J. P. D. (1968). "A penetration criterion for double-walled structures subject to meteoroid impact." *AIAA J.*, 7(10), 1937–1943.
Zukas, J. A., et al. (1982). *Impact dynamics*. John Wiley and Sons, New York, N.Y.

APPENDIX II. NOTATION

The following symbols are used in this paper:

C = speed of sound in bumper plate material;
D = normal impact bumper plate hole dimension;
D_{max} = maximum bumper plate hole dimension;
D_{min} = minimum bumper plate hole dimension;
d = projectile diameter;
t_s = bumper plate thickness;
V = impact velocity;
α_c = angle subtending 50% of ricochet debris particle trajectories;
α_{99} = angle subtending 99% of ricochet debris particle trajectories;
γ_1 = angular spread of bumper plate debris cloud;
γ_2 = angular spread of projectile fragments debris cloud;
θ = impact trajectory obliquity;
θ_1 = bumper plate debris center-of-mass trajectory; and
θ_2 = projectile fragments center-of-mass trajectory.